Local frequency density of states around field inhomogeneities in magnetic resonance imaging: Effects of diffusion

C. H. Ziener,[1] T. Kampf,[1] G. Melkus,[1] V. Herold,[1] T. Weber,[1] G. Reents,[2] P. M. Jakob,[1] and W. R. Bauer[3]
[1]*Julius-Maximilians-Universität Würzburg, Lehrstuhl für Experimentelle Physik 5, Am Hubland, 97074 Würzburg, Germany*
[2]*Julius-Maximilians-Universität Würzburg, Institut für Theoretische Physik, Am Hubland, 97074 Würzburg, Germany*
[3]*Julius-Maximilians-Universität Würzburg, Medizinische Universitätsklinik, Josef-Schneider-Strasse 2, 97080 Würzburg, Germany*
(Received 18 December 2006; revised manuscript received 27 April 2007; published 14 September 2007)

A method describing NMR-signal formation in inhomogeneous tissue is presented which covers all diffusion regimes. For this purpose, the frequency distribution inside the voxel is described. Generalizing the results of the well-known static dephasing regime, we derive a formalism to describe the frequency distribution that is valid over the whole dynamic range. The expressions obtained are in agreement with the results obtained from Kubos line-shape theory. To examine the diffusion effects, we utilize a strong collision approximation, which replaces the original diffusion process by a simpler stochastic dynamics. We provide a generally valid relation between the frequency distribution and the local Larmor frequency inside the voxel. To demonstrate the formalism we give analytical expressions for the frequency distribution and the free induction decay in the case of cylindrical and spherical magnetic inhomogeneities. For experimental verification, we performed measurements using a single-voxel spectroscopy method. The data obtained for the frequency distribution, as well as the magnetization decay, are in good agreement with the analytic results, although experiments were limited by magnetic field gradients caused by an imperfect shim and low signal-to-noise ratio.

DOI: 10.1103/PhysRevE.76.031915 PACS number(s): 87.61.−c, 33.25.+k, 76.60.−k

I. INTRODUCTION

The signal intensity in magnetic resonance imaging arises mainly from spin density and longitudinal and transverse relaxation. The transverse relaxation is especially sensitive to the magnetic properties of tissue, which is often composed of structures with different magnetic susceptibility. In the presence of an external magnetic field, these structures induce an inhomogeneous field which accelerates the transverse relaxation. Important examples where this susceptibility effect plays a role are functional imaging of the brain [1] and cell tracking [2–4]. The first depends on the paramagnetic property of deoxyhemoglobin, which then acts as a natural contrast agent; the second uses external contrast agents, e.g., ultrasmall superparamagnetic contrast agents (USPIOs), to label cells like macrophages or stem cells [5]. At present, these susceptibility-sensitive imaging techniques mainly provide qualitative information about the tissue structures, e.g., capillaries and cells. However, one paramount goal is to also obtain quantitative data, e.g., what the capillary density is [6,7] or how many cells are in a specific voxel [8]. To achieve this, models are needed which relate the signal intensity to these relevant structures. This information is comprised in the time evolution of the magnetization decay or, what is equivalent, in its frequency spectrum. For example, in a recent work we demonstrated that the volume fraction of a capillary inside a voxel could be determined by the frequency distribution around the capillary (cf. Fig. 3 in [9]). Zhong *et al.* used these results to describe the signal formation in the human visual cortex by applying a balanced steady-state free precession (SSFP) sequence [10].

The motivation for this investigation is that for the abovementioned problems the question arises: which sequence to use with which parameters. The first step to answering this question is to characterize the tissue by the frequency distribution caused by the enclosed field inhomogeneities. For a given arrangement the frequency distribution exhibits a typical form which is dependent on the susceptibility difference between the magnetized object and the surrounding medium, the strength of the external magnetic field, and the volume fraction of material inside the voxel. Detailed knowledge of this form allows one to choose the magnetic resonant imaging (MRI) sequence with parameters optimized to obtain information about the tissue properties which influence the frequency distribution.

The intensity in an image taken by NMR techniques corresponds to the averaged signal from a three-dimensional volume element called a voxel. Therefore, it is necessary to understand the signal formation inside these voxels. The size of such a voxel can vary from the millimeter down to the micrometer range. As illustrated in Fig. 1, such a voxel may contain small magnetic inhomogeneities that cannot be resolved by MRI such as blood-filled capillaries or air-filled alveols. These inhomogeneities generate an inhomogeneous local magnetic field $B_z(\mathbf{r})$ depending on the shape of the magnetic perturber, but can be modeled by cylinders or spheres. Via the Larmor relation $\omega(\mathbf{r})=\gamma B_z(\mathbf{r})$, the local field strength is connected to a local resonance frequency $\omega(\mathbf{r})$ inside a voxel. To understand the signal formation process, it is convenient to introduce the frequency distribution $p(\omega)$, which is closely connected to the local Larmor frequency in the sense that it is a density of states. The second quantity which influences the signal formation is the pulse sequence used, which causes a distinct excitation of different local Larmor frequencies ω. The NMR signal is the induced voltage in a receiver coil caused by the precession of the magnetization vector around the axis of the external magnetic field in the z direction. Hence, the excitation strength for each local frequency is the transverse magnetization $M_x(\omega)+iM_y(\omega)$, which is also called the response function of the

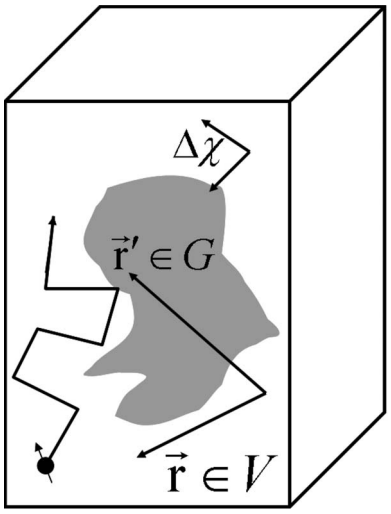

FIG. 1. Voxel with the volume V_{voxel} containing a magnetic inhomogeneity G and the remaining dephasing volume V. The inhomogeneity G generates the susceptibility difference $\Delta\chi$ to the surrounding medium with the diffusion coefficient D in which the diffusion of the nuclear spins occurs.

sequence and depends on the sequence of rf pulses applied. Therefore, the average signal from a voxel can be expressed as an integral over all local frequencies in the form [11–14]

$$M(t) = \int_{-\infty}^{+\infty} p(\omega)[M_x(\omega) + iM_y(\omega)]e^{i\omega t}d\omega. \qquad (1)$$

To illustrate this signal formation process, examples of the relevant quantities are shown in Fig. 2. In the case of a gradient-echo sequence [fast low angle shot (FLASH) [15]], the response function is a constant, $M_x(\omega)+iM_y(\omega)=$const. Thus, the time evolution of the signal is the Fourier transformation of the frequency distribution, which can be easily obtained from Eq. (1). Hence, we can state that the frequency distribution is equivalent to the static inhomogeneous spectroscopic line shape of a free induction decay. As an illustration, we show a Lorentzian line shape for the frequency distribution in Fig. 2. The actual shape of the frequency distribution depends on the form of the field inhomogeneity and the diffusion in the surrounding medium. The effect of different line shapes on the time evolution of an NMR signal has been studied in detail in the case of a SSFP sequence by Ganter [17]. The topic of this work is to give an analytical approach to calculating this distribution and its experimental verification.

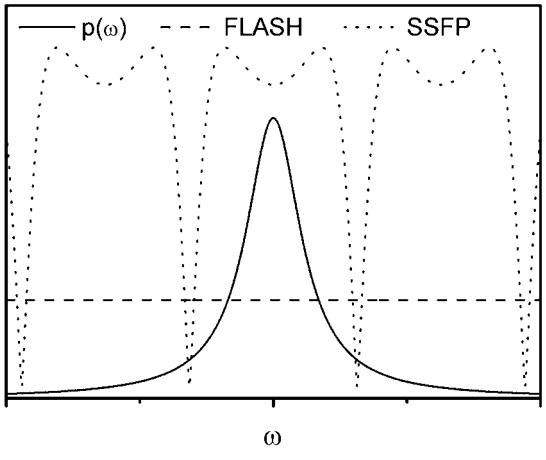

FIG. 2. Quantities that influence the signal formation inside a voxel according to Eq. (1). The response function $M_x(\omega)+iM_y(\omega)$ is sequence specific and used to describe the offresonance behavior of these sequences (dashed line for a FLASH sequence [15] and dotted line for a SSFP sequence [16]). A Lorentzian frequency distribution $p(\omega)$ is shown by the solid line.

One way to obtain the time evolution of the magnetization is by solving the Bloch-Torrey equation directly. Including diffusion, this is cumbersome and analytical approaches work only in special cases, e.g., when $\omega(\mathbf{r})$ is the frequency of a linear gradient field [18–20]. Alternatively, it is possible to solve the Bloch-Torrey equation numerically. For example, this was applied to describe the effect of edge enhancement by diffusion [21–23] by applying the line-shape theory of Kubo [24,25]. Another method to describe the transverse relaxation was recently presented by Kiselev, Posse, and Novikov [26–28]. They used analytical models for very long and short correlation times. The first extends the static dephasing regime and the second is a perturbation approach in the local magnetic field. However, these results are limited to special cases, which limits their range of application. An approach that describes spin dephasing over the whole dynamic range is the Gaussian approximation [29–31], which works as long as the stochastic dynamics are restricted to a limited class [32]. A solution of the Bloch-Torrey equation is also well approximated by the (extended) *strong collision approximation* [33]. In order to consider the non-Gaussian character of diffusion, the results of this approximation will be used throughout this work.

This work focuses on another way to access this problem. Different parameters influence the signal obtained from a voxel containing inhomogeneous magnetic fields. As can be seen from Eq. (1), both the sequence used, with its parameters [represented by $M_x(\omega)+iM_y(\omega)$], and the distribution of field inhomogeneities inside the tissue [represented by $p(\omega)$] influence the signal arising from the voxel. To obtain information about the signal evolution, we focus on the frequency distribution.

In previous work, the frequency distribution was evaluated in the static dephasing regime in which diffusion effects are neglected. In the case of a homogeneous magnetized sphere in the center of a voxel, the frequency distribution exhibits a single peak [34]. The frequency distribution of a cylindrical inhomogeneity inside a voxel shows a characteristic shape with two peaks, while randomly distributed cylinders lead to a Lorentzian-like distribution [9].

While the static dephasing regime is well understood [11,35], the influence of diffusion of the water molecules around the inhomogeneities is an important factor which influences the frequency distribution and must be taken into account [36]. In this work, we give a rigorous deduction of the frequency distribution inside a voxel with respect to the shape of the particles generating the susceptibility differ-

ences as well as the diffusion around these particles. To describe the diffusion process, a *strong collision approximation* is applied which approximates the diffusion dynamics of spins by simpler stochastic dynamics. Thus, it is possible to deduce a formalism to describe the frequency distribution around arbitrarily shaped field inhomogeneities.

First, in Sec. II we consider some general aspects of signal formation in nuclear magnetic resonance which are necessary for the following work. Afterwards, coming from the theory of the static dephasing regime, the expression of the frequency distribution is extended to all diffusion regimes. The limiting cases of motional narrowing and the static dephasing regime are recovered by the appropriate limiting procedures from the general result. This theory is applicable to arbitrary geometries which can be evaluated numerically or analytically. To demonstrate this procedure, the analytical expressions for spherical and cylindrical inhomogeneities are calculated in Sec. III. The experimental verification of the analytical results is presented in Sec. IV. A summary and conclusions are then given in Sec. V. A detailed description of the approximation used and some remarks on the connection to Kubos line-shape theory are given in the Appendix.

II. GENERAL THEORY

From the general theory of NMR-signal formation, it is known that the time evolution of the magnetization is completely determined by both the frequency distribution inside the voxel and the response function of the NMR-pulse sequence used [cf. Eq. (1)]. While the effects of diffusion on the response function are well understood [37–39], the frequency distribution has only been investigated in the static dephasing regime [9,34]. Thus, the topic of this work is to obtain a general expression for the frequency distribution which is valid for all diffusion regimes.

A. Spin dephasing inside a voxel

In this part, an outline of the formation of the NMR signal is presented. To this end, we give a short review of the ideas behind the strong collision approximation required to deduce the frequency distribution at all diffusion regimes. As is well known, the NMR signal arises from the transverse magnetization inside a voxel. To describe its time evolution, we consider a single voxel with volume $V_{\text{voxel}}=V+G$, as shown in Fig. 1. A magnetic inhomogeneity with volume G is located inside this voxel and surrounded by tissue with a constant diffusion coefficient D and volume V where the diffusion and dephasing of spins take place. Thus, it is possible to introduce the volume fraction of the inhomogeneity, $\eta=G/V_{\text{voxel}}$. The inhomogeneity generates a susceptibility shift $\Delta\chi$ leading to an inhomogeneous magnetic field $B_z(\mathbf{r})$ and thus a spatially varying Larmor frequency $\omega(\mathbf{r})$ inside the voxel. As shown in [40,41], this local frequency is given by

$$\omega(\mathbf{r}) = \delta\omega \frac{\partial^2}{\partial z^2} \int_G \frac{d^3\mathbf{r}'}{|\mathbf{r}-\mathbf{r}'|}, \tag{2}$$

where $\delta\omega=\gamma\Delta\chi B_0$ characterizes the frequency shift caused by the magnetic field inhomogeneity.

To describe the time evolution of the dephasing of the transverse part of the magnetization vector, we assume that for all diffusion regimes the Bloch-Torrey equation [18]

$$\frac{\partial}{\partial t} m(\mathbf{r},t) = [D\nabla^2 + i\omega(\mathbf{r})] m(\mathbf{r},t) \tag{3}$$

is valid. The local frequency $\omega(\mathbf{r})$ is given in Eq. (2) and depends on the form of the macroscopic field inhomogeneity only. Here, $m(\mathbf{r},t)=m_x(\mathbf{r},t)+im_y(\mathbf{r},t)$ is the magnetization which is generated at point $\mathbf{r}$ in polar form. Since we are interested in the effect of the susceptibility-induced macroscopic field inhomogeneity, we focus our investigation on this effect. For this reason, other terms of the full Bloch-Torrey equation [42] are neglected.

In NMR experiments, only the signal emitted from the whole voxel can be measured. Thus, we focus on the average magnetization of the voxel which is given by

$$M(t) = \frac{1}{V} \int_V d^3\mathbf{r} m(\mathbf{r},t). \tag{4}$$

To solve the Bloch-Torrey equation (3), we will describe the diffusion process in the sense of transition dynamics. Due to diffusion through the local inhomogeneous magnetic field, the spin is exposed to different Larmor frequencies $\omega(\mathbf{r})$ at different times. This diffusion process is exclusively characterized by the correlation time τ, which depends on the form and size of the perturber, and the diffusion coefficient D [41,43] and can be written in terms of the local Larmor frequency

$$\tau = \frac{1}{\langle\omega^2(\mathbf{r})\rangle DV} \int_V d^3\mathbf{r}\omega(\mathbf{r}) \left[-\frac{1}{\nabla^2}\right] \omega(\mathbf{r}), \tag{5}$$

where $\langle\omega^2(\mathbf{r})\rangle = 1/V\int_V d^3\mathbf{r}\omega^2(\mathbf{r})$. The influence of the susceptibility effects and the strength of the external magnetic field determine the static frequency $\delta\omega \propto \Delta\chi B_0$. On the contrary, the diffusion is described by the correlation time, which induces the dynamic frequency $1/\tau$ of field fluctuations. Comparison of both of the frequencies determines the underlying diffusion regime [44]. If the diffusion can be neglected, i.e., $\delta\omega \gg 1/\tau$, the static dephasing regime holds, whereas in the opposite case $\delta\omega \ll 1/\tau$, the approximations of the motional narrowing regime can be applied.

If the time scale of the diffusion τ is well separated from the time scale of dephasing, i.e., $\tau \ll T_2^*$, one can assume that diffusion and dephasing are described by stochastically independent processes. These separated time scales lead to the effect that every spin diffusing around the inhomogeneity covers nearly all off-resonance frequencies with a probability according to their occurrence in the frequency distribution. From this point of view, the spin ensemble can be described as an ergodic system. This occurs on the time scale of the correlation time τ. Hence, the time scale on which the local Larmor frequencies are correlated is much smaller than the time scale of the dephasing related to the susceptibility effects of the field inhomogeneity. With this in mind, the original diffusion process can be considered as a stationary Markov process and the diffusion operator $D\nabla^2$ can be replaced

by the strong collision operator **D** (for details see the Appendix). Thus, the strong collision approximation will work well in the motional narrowing regime which is characterized by the above assumption. On the other hand, the equilibrium transition dynamics are also exact in the case of nondiffusing spins $\tau \to \infty$ [cf. Eqs. (A3) and (A8)]. In this case, the equilibrium distribution of spins is given at all times and the diffusion operator can be replaced by the strong collision operator, in the sense that both operators vanish. From this point of view, the strong collision approximation can be considered as an interpolation between both limiting diffusion regimes and will be used to describe the influence of diffusion over the whole dynamic range.

As shown in the Appendix, it is convenient to introduce the Laplace transformation of the magnetization time evolution in the form

$$\hat{M}(s) = \int_0^\infty dt\, e^{-st} M(t). \tag{6}$$

Throughout this work, quantities in the static dephasing regime will be labeled with the subscript zero [i.e., the time evolution of the magnetization in the static dephasing regime $M_0(t)$ corresponds to the Laplace transformation $\hat{M}_0(s)$]. In order to generalize the static dephasing results to arbitrary diffusion regimes via the correlation time τ, we derive in the Appendix the expression

$$\hat{M}(s) = \frac{\hat{M}_0(s+\tau^{-1})}{1-\tau^{-1}\hat{M}_0(s+\tau^{-1})}. \tag{7}$$

This is the crucial result of the strong collision approximation and will be utilized in the course of this work to extend the frequency distribution to all diffusion regimes.

B. Static dephasing regime

As shown previously, the results of the static dephasing limit can be extended in a simple way to cover all diffusion regimes by considering the Laplace transformation of the relevant quantities (7). Hence, the ability to calculate all quantities in the static dephasing regime is imperative. The static dephasing regime is characterized by $D=0$; therefore, the signal from a voxel is given by

$$M_0(t) = \frac{1}{V}\int_V d^3\mathbf{r}\rho(\mathbf{r}) e^{i\omega(\mathbf{r})t}, \tag{8}$$

where V is the dephasing volume, $\omega(\mathbf{r})$ is the local Larmor frequency, and $\rho(\mathbf{r})$ is the spin density [11,34,35,45]. For the spin density, we assume $\rho(\mathbf{r})=\rho=$const throughout the whole voxel. On the other hand, the signal can be written in terms of frequency distribution in the form

$$M_0(t) = \rho\int_{-\infty}^{+\infty} d\omega p_0(\omega) e^{i\omega t}. \tag{9}$$

Adapting methods of statistical physics [9,34,46], we are able to define a frequency density of states. Therefore we equate Eqs. (8) and (9):

$$\int_{-\infty}^{+\infty} d\omega p_0(\omega) e^{i\omega t} = \frac{1}{\rho V}\int_V d^3\mathbf{r}\rho(\mathbf{r}) e^{i\omega(\mathbf{r})t}. \tag{10}$$

Performing an inverse Fourier transformation and using the definition of the Dirac distribution one can write the frequency distribution in the following way:

$$p_0(\omega) = \frac{1}{\rho V}\int_V d^3\mathbf{r}\rho(\mathbf{r})\delta[\omega-\omega(\mathbf{r})], \tag{11}$$

which has the properties of a probability density

$$\int_{-\infty}^{+\infty} d\omega p_0(\omega) = 1, \quad p_0(\omega) \geqslant 0. \tag{12}$$

This frequency density of states is equivalent to the static inhomogeneous spectroscopic line shape of a free induction decay and is also known as an off-resonance frequency distribution in the field of magnetic resonance imaging. The term density of states is used to show the close connection to statistical physics which enables the use of the methods used in this field.

Using the Fourier representation of the Dirac δ distribution, the integral (11) can, in principle, be evaluated analytically for any given local Larmor frequency $\omega(\mathbf{r})$. For complicated geometries, the frequency distribution can be determined numerically by dividing the dephasing volume V into small subvoxels and averaging the Larmor frequency in each of them. The frequency distribution is then the histogram of the number of subvoxels according to the Larmor frequencies. However, this method cannot include diffusion effects. Therefore, another way to calculate the diffusion-dependent frequency distribution will be shown in the next subsection.

For this purpose, we will utilize Eq. (7) which connects the static dephasing results with all other diffusion regimes. Therefore, it is necessary to know the Laplace transformation of the magnetization time decay in the static dephasing regime and its connection to the other relevant quantities:

$$\hat{M}_0(s) = \int_0^\infty dt\, e^{-st} M_0(t) \tag{13}$$

$$= \rho\int_{-\infty}^{+\infty} d\omega \frac{p_0(\omega)}{s+i\omega} \tag{14}$$

$$= \rho\int_V d^3\mathbf{r}\frac{1}{s-i\omega(\mathbf{r})}, \tag{15}$$

which can be easily deduced using properties of the Laplace transformation.

C. Extension to all diffusion regimes

To find an expression for the frequency distribution it is convenient to start with a generalization of Eq. (9) to all diffusion regimes where the signal can be written as a Fourier transformation of the frequency distribution

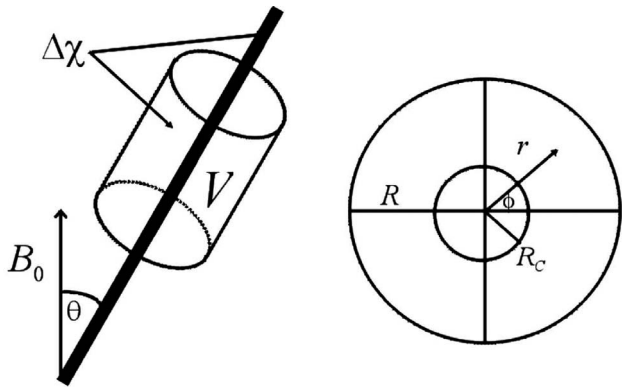

FIG. 3. Left side: cylinder with a tilt angle θ to the external magnetic field B_0. According to Krogh's capillary model, the cylinder is surrounded by a cylindrical voxel. The dephasing occurs in the remaining volume V. Right side: cross-sectional view of the cylinder and the coaxial surrounding voxel with the polar coordinates r and ϕ. The radius of the cylinder is denoted as R_C, the radius of the voxel as R.

$$M(t) = \rho \int_{-\infty}^{+\infty} d\omega p(\omega) e^{i\omega t}. \tag{16}$$

The frequency distribution is given by the inverse Fourier transformation in the following way:

$$p(\omega) = \frac{1}{2\pi\rho} \int_{-\infty}^{+\infty} dt\, e^{-i\omega t} M(t) \tag{17}$$

$$= \frac{1}{2\pi\rho} |\hat{M}(i\omega) + \hat{M}^*(i\omega)| \tag{18}$$

$$= \frac{1}{\pi\rho} |\mathrm{Re}\, \hat{M}(i\omega)|, \tag{19}$$

where $\hat{M}(s)$ is the Laplace transformation of the magnetization time evolution. Up until this point, no approximation has been applied. For calculating the Laplace transformation, we introduce the crucial result of the strong collision approximation (7) in Eq. (19) and obtain

$$p(\omega) = \frac{1}{\pi\rho} \left| \mathrm{Re}\, \frac{\hat{M}_0(i\omega + \tau^{-1})}{1 - \tau^{-1} \hat{M}_0(i\omega + \tau^{-1})} \right|. \tag{20}$$

To find a connection between the frequency distribution $p(\omega)$ and the local Larmor frequency $\omega(\mathbf{r})$, we utilize the relationship between the Laplace transformation $\hat{M}_0(s)$ and $\omega(\mathbf{r})$ given in Eq. (15). Setting $s = i\omega + \tau^{-1}$ in Eq. (15) and inserting in the above equation, we eventually arrive at

$$p(\omega) = \frac{\tau}{\pi} \left| \mathrm{Re} \left\{ \left[\int_V \frac{d^3\mathbf{r}}{1 + i\tau[\omega - \omega(\mathbf{r})]} \right]^{-1} - \rho \right\}^{-1} \right|. \tag{21}$$

This final expression is the generalization of Eq. (11) for all diffusion regimes. It depends on the correlation time and the local Larmor frequency only. Although it has a quite simple structure, analytical solutions are only available in special cases of the geometry of the magnetic inhomogeneity G and the dephasing volume $V = V_{\mathrm{voxel}} - G$.

From Eq. (7), we obtain in the limit of small correlation times $\lim_{\tau \to 0} \hat{M}(s) = \rho/s$, which leads to a δ peak according to the motional narrowing limit $\lim_{\tau \to 0} p(\omega) = \delta(\omega)$. As expected, in the limit of nonmoving spins, all observables tend to their static dephasing limit, i.e., $\lim_{\tau \to \infty} \hat{M}(s) = \hat{M}_0(s)$, which leads to the static dephasing frequency density of states given in Eq. (11), i.e., $\lim_{\tau \to \infty} p(\omega) = p_0(\omega)$.

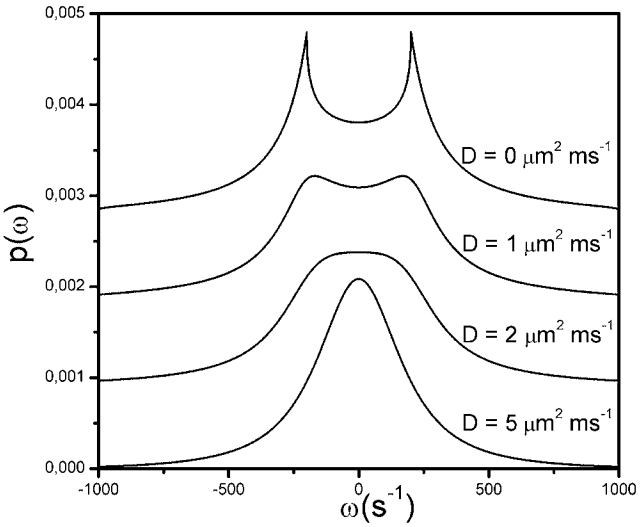

FIG. 4. Diffusion-dependent frequency density of states $p(\omega)$ for cylinders obtained from Eq. (50) using the cylinder H function given in Eq. (35). The parameters are volume fraction $\eta = 0.2$, equatorial frequency shift $\delta\omega_\theta = 1000\ \mathrm{s}^{-1}$, and radius $R_C = 5\ \mu\mathrm{m}$.

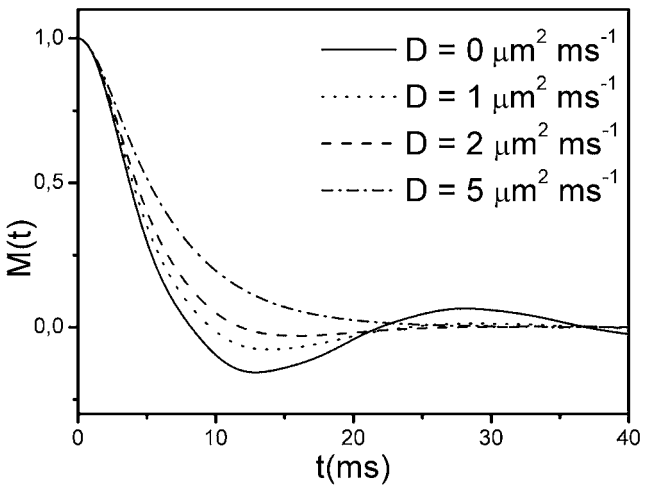

FIG. 5. Diffusion-dependent signal decay $M(t)$ for cylinders obtained by a Fourier transformation of the frequency density of states $p(\omega)$ according to Eq. (16). The parameters are volume fraction $\eta = 0.2$, equatorial frequency shift $\delta\omega_\theta = 1000\ \mathrm{s}^{-1}$, and radius $R_C = 5\ \mu\mathrm{m}$.

Until now, only gradient echo sequences have been considered. In order to describe the magnetization time evolution of a classical Hahn-spin-echo experiment, $M_{\mathrm{SE}}(t)$ [47], we start from the results of a gradient echo sequence. Knowing the free induction decay of the gradient echo sequence $M(t)$ given in Eq. (16), according to [48], we are able to obtain the spin-echo magnetization time evolution

$$M_{\mathrm{SE}}(t) = e^{-t/\tau} + \frac{e^{-t/\tau}}{\tau}\int_0^t d\xi\, e^{\xi/\tau}\left|M\left(\frac{\xi}{2}\right)\right|^2. \tag{22}$$

III. APPLICATION TO INHOMOGENEOUS TISSUES

The general theory derived in the previous section can be used to obtain the frequency distribution $p(\omega)$ for any diffusion regime around a magnetic inhomogeneities of arbitrary shape. In order to obtain analytical expressions for the frequency distribution, we assume that the shape of the voxel is the same as the shape of the magnetic inhomogeneity; i.e., the voxel arises from the magnetic inhomogeneity by a central dilation. This means, for example, that for a cylindrical magnetic inhomogeneity, the voxel has the shape of a cylinder (see Fig. 3). The well-known Krogh capillary model [49], where a cylindrical capillary is surrounded by a cylindrical volume of tissue, is adapted in this case. Assuming the volume fraction $\eta = G/V_{\mathrm{voxel}}$ fulfills the condition $\eta \ll 1$, the actual shape of the voxel is irrelevant and the result is the same as for a cuboid voxel of the same volume [9,35]. In the next subsections, we demonstrate the formalism for cylindrical and spherical inhomogeneities. In the case of small volume fraction η these special results can easily be generalized to arbitrary shaped objects.

A. Cylinders

As a first example which can be solved analytically, we consider a cylinder which has a tilt angle θ to an external magnetic field B_0. The cylinder generates the susceptibility difference $\Delta\chi$ to the surrounding tissue, which leads to the inhomogeneous magnetic field

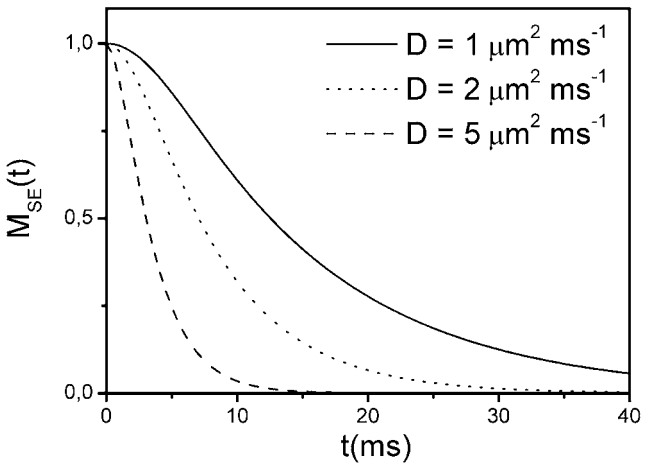

FIG. 6. Diffusion-dependent spin-echo signal decay $M_{\mathrm{SE}}(t)$ for cylinders obtained from Eq. (22) with the gradient-echo magnetization decay $M(t)$ shown in Fig. 5. The parameters are volume fraction $\eta=0.2$, equatorial frequency shift $\delta\omega_\theta = 1000\ \mathrm{s}^{-1}$, and radius $R_{\mathrm{C}} = 5\ \mu\mathrm{m}$.

$$B(\mathbf{r}) = \frac{\Delta\chi}{2} B_0 \sin^2\theta\, R_{\mathrm{C}}^2 \frac{\cos 2\phi}{r^2}, \tag{23}$$

where (r,ϕ) are the polar coordinates in the cross-sectional view (see Fig. 3) [50]. Introducing the characteristic equatorial frequency shift

$$\delta\omega_\theta = \gamma B(r = R_{\mathrm{C}}, \phi = 0) \tag{24}$$

$$= \gamma \frac{\Delta\chi}{2} B_0 \sin^2\theta, \tag{25}$$

where γ is the gyromagnetic ratio, we have

$$\omega_{\mathrm{C}}(\mathbf{r}) = \delta\omega_\theta R_{\mathrm{C}}^2 \frac{\cos 2\phi}{r^2}. \tag{26}$$

As described above, we assume the cylinder with radius R_{C} to be surrounded by a concentric cylindrical voxel with radius R. In this case, the dephasing volume V is the space between the two concentric cylinders with radii R_{C} and R. Performing the integration in Eq. (11) using the local frequency (26) yields [see Eq. (9) in [9]]

$$p_{0,\mathrm{C}}(\omega) = \begin{cases} \dfrac{\eta}{1-\eta}\dfrac{\delta\omega_\theta}{\pi\omega^2}\sqrt{1-\left(\dfrac{\omega}{\delta\omega_\theta}\right)^2} & \text{for } \omega \leqslant -\eta\delta\omega_\theta \text{ or } \omega \geqslant \eta\delta\omega_\theta, \\ \dfrac{\eta}{1-\eta}\dfrac{\delta\omega_\theta}{\pi\omega^2}\left[\sqrt{1-\left(\dfrac{\omega}{\delta\omega_\theta}\right)^2} - \sqrt{1-\left(\dfrac{\omega}{\eta\delta\omega_\theta}\right)^2}\right] & \text{for } -\eta\delta\omega_\theta \leqslant \omega \leqslant \eta\delta\omega_\theta, \\ 0 & \text{otherwise,} \end{cases} \tag{27}$$

where $\eta = R_{\mathrm{C}}^2/R^2$ is the volume fraction $(0 \leqslant \eta \leqslant 1)$ of the cylinder inside the voxel. Introducing this static dephasing frequency density of states (27) into the Fourier transformation (9), we obtain an expression for the magnetization decay in the static dephasing regime:

$$M_0(t) = \frac{\rho}{1-\eta}\left[{}_1F_2\left\{ \begin{matrix} -\frac{1}{2} \\ \frac{1}{2}, \quad 1 \end{matrix} \middle| -\left(\frac{\eta\delta\omega_\theta t}{2}\right)^2 \right\} - \eta\, {}_1F_2\left\{ \begin{matrix} -\frac{1}{2} \\ \frac{1}{2}, \quad 1 \end{matrix} \middle| -\left(\frac{\delta\omega_\theta t}{2}\right)^2 \right\} \right], \tag{28}$$

where the generalized hypergeometric function or Barnes extended hypergeometric function is defined as [51]

$${}_pF_q\left\{ \begin{matrix} a_1, \ldots, a_p \\ b_1, \ldots, b_q \end{matrix} \middle| z \right\} = \sum_{k=0}^{\infty} \frac{(a_1)_k (a_2)_k \cdots (a_p)_k}{(b_1)_k (b_2)_k \cdots (b_q)_k} \frac{z^k}{k!} \tag{29}$$

and the Pochhammer is symbol given by

$$(x)_k = \frac{\Gamma(x+k)}{\Gamma(x)}. \tag{30}$$

Alternatively, the magnetization decay in the static dephasing regime $M_0(t)$ can be obtained by introducing the frequency field $\omega_C(\mathbf{r})$ given in Eq. (26) into the general expression (8).

Obviously, the magnetization decay in Eq. (28) can be expressed in the form

$$M_0(t) = \frac{\rho}{1-\eta}[h_C(\eta\delta\omega_\theta t) - \eta h_C(\delta\omega_\theta t)], \tag{31}$$

with the cylinder-specific h function

$$h_C(x) = {}_1F_2\left\{ \begin{matrix} -\frac{1}{2} \\ \frac{1}{2}, \quad 1 \end{matrix} \middle| -\left(\frac{x}{2}\right)^2 \right\}, \tag{32}$$

which corresponds to the function $g(x)$ given in Eq. (13) of [9]. In order to obtain the frequency distribution in all diffusion regimes, it is necessary to start with the calculation of the Laplace transformation of the magnetization decay in the static dephasing regime $\hat{M}_0(s)$ with the help of one of the equations (13)–(15). All of them lead to the same result for the Laplace transformation of the magnetization decay $\hat{M}_0(s)$:

$$\hat{M}_0(s) = \frac{\rho}{1-\eta}\frac{1}{s}\left[\sqrt{1 + \frac{\eta^2\delta\omega_\theta^2}{s^2}} - \eta\sqrt{1 + \frac{\delta\omega_\theta^2}{s^2}} \right]. \tag{33}$$

To abbreviate this expression, we rewrite the Laplace transformation in close analogy to Eq. (31) in the form

$$\hat{M}_0(s) = \frac{\rho}{1-\eta}\frac{1}{s}\left[H_C\left(\frac{s}{\eta\delta\omega_\theta}\right) - \eta H_C\left(\frac{s}{\delta\omega_\theta}\right) \right], \tag{34}$$

with the cylinder specific function

$$H_C(y) = \sqrt{1 + \frac{1}{y^2}}. \tag{35}$$

To calculate the Laplace transformation of the magnetization valid in all diffusion regimes, we have to introduce Eq. (34) into Eq. (7). The resulting Laplace transformation $\hat{M}(s)$ has to be inserted into Eq. (19), and we eventually arrive at

$$p(\omega) = \frac{\tau_C}{\pi\rho}\left| \mathrm{Re}\, \frac{H_C\left(\frac{1+i\tau_C\omega}{\eta\tau_C\delta\omega_\theta}\right) - \eta H_C\left(\frac{1+i\tau_C\omega}{\tau_C\delta\omega_\theta}\right)}{\frac{1-\eta}{\rho}(1+i\tau_C\omega) - H_C\left(\frac{1+i\tau_C\omega}{\eta\tau_C\delta\omega_\theta}\right) + \eta H_C\left(\frac{1+i\tau_C\omega}{\tau_C\delta\omega_\theta}\right)} \right|. \tag{36}$$

This expression is the frequency density of states for cylindrical geometries which depends on the diffusion (characterized by the correlation time τ_C), the susceptibility effect (characterized by the frequency shift $\delta\omega_\theta$), and the shape of the magnetized object (characterized by the function H_C). An expression for the frequency distribution equal to Eq. (36) is obtained if the local resonance frequency given in Eq. (26) is directly inserted in the general expression (21).

In order to calculate the frequency distribution with the help of Eq. (36), it is necessary to determine the correlation time τ_C that describes the diffusion effects. In the case of a nonpermeable cylinder, we assume reflecting boundary conditions on the surface of the inner cylinder. In this case, the

correlation time can be obtained by evaluating the general expression in Eq. (5) as shown in [6,43]:

$$\tau_C = -\frac{R_C^2}{4D}\frac{\ln \eta}{1-\eta}. \tag{37}$$

To illustrate the dependence on the diffusion, the frequency density of states is shown in Fig. 4 for different values of the diffusion coefficient D. In the case of a vanishing diffusion coefficient the frequency density of states coincides with the static dephasing frequency distribution given in Eq. (27) and is shown in Fig. 1 of [9]. A similar characteristic form of the frequency distribution was obtained by Zimmermann and Foster numerically for cylindrical geometries [52]. In the case of an increasing diffusion coefficient D, the frequency distribution tends to a single-peaked narrow line shape which is expected in the motional narrowing regime, as can be seen from Fig. 4.

A Fourier transformation of the frequency density of states $p(\omega)$ according to Eq. (16) leads to the magnetization decay shown in Fig. 5. Also, here in the static dephasing regime, the magnetization decay coincides with the former results given in Eq. (31) using the cylinder-specific function (32), as shown in Fig. 2 of [9]. The spin-echo signal decay can be obtained from Eq. (22) and is shown in Fig. 6.

B. Spheres

The second case which is possible to solve analytically is a homogeneous magnetized sphere in an external magnetic field. The frequency density of states and signal properties in the static dephasing regime were extensively studied by Cheng *et al.* [34] analytically. The experimental verification was performed by Seppenwoolde *et al.* [53]. The case of spheres has also been treated numerically to investigate signal formation in lung tissue, where the alveolus is modeled by a sphere surrounded by a water-filled shell [54–57]. The application of the static dephasing regime to the problem of signal formation around superparamagnetic iron-oxide-labeled cells was treated by Bowen *et al.* [58]. As mentioned in Sec. II B, they obtained the frequency distribution in terms of a histogram.

The frequency around a sphere with the radius R_S is the field of a dipole given by

$$\omega_S(\mathbf{r}) = \delta\omega R_S^3 \frac{3\cos^2\theta - 1}{r^3}, \tag{38}$$

where $\delta\omega$ is the characteristic frequency shift and θ is the angle between the external magnetic field B_0 and the position vector $\mathbf{r}$. Analogously to the case of cylinders, we assume the sphere to be located in the center of a spherical voxel with the radius R. Performing the integration in Eq. (11) using the local frequency (38), the static dephasing frequency density of states is given by [34]

$$p_{0,S}(\omega) = \begin{cases} \dfrac{\eta}{3\sqrt{3}(1-\eta)}\left(\dfrac{\delta\omega}{\omega}\right)^2\left(2-\dfrac{\omega}{\delta\omega}\right)\sqrt{1+\dfrac{\omega}{\delta\omega}} & \text{for } \omega \leqslant -\eta\delta\omega_\theta \text{ or } \omega \geqslant 2\eta\delta\omega_\theta, \\ \dfrac{\eta}{3\sqrt{3}(1-\eta)}\left(\dfrac{\delta\omega}{\omega}\right)^2\left[\left(2-\dfrac{\omega}{\delta\omega}\right)\sqrt{1+\dfrac{\omega}{\delta\omega}} - \left(2-\dfrac{\omega}{\eta\delta\omega}\right)\sqrt{1+\dfrac{\omega}{\eta\delta\omega}}\right] & \text{for } -\eta\delta\omega_\theta \leqslant \omega \leqslant 2\eta\delta\omega_\theta, \\ 0 & \text{otherwise}, \end{cases} \tag{39}$$

where $\eta = R_S^3/R^3$ is the volume fraction ($0 \leqslant \eta \leqslant 1$). Introducing this static dephasing frequency density of states (39) into the Fourier transformation (9) or evaluating the integral (8), the magnetization time evolution can be written as in the cylindrical case (31) as

$$M_0(t) = \frac{\rho}{1-\eta}[h_S(\eta\delta\omega t) - \eta h_S(\delta\omega t)], \tag{40}$$

with the sphere-specific h function

$$h_S(x) = e^{-ix}\,{}_1F_1\left(\left.\begin{matrix}\frac{1}{2} \\ \frac{3}{2}\end{matrix}\right| 3ix\right) + \int_0^1 dz\, x(3z^2-1)[\mathrm{Si}(x(3z^2-1)) - i\,\mathrm{Ci}(x|3z^2-1|)]. \tag{41}$$

The Kummer confluent hypergeometric function ${}_1F_1$ is the special case of Barnes extended hypergeometric function (29) for $p=1=q$ and the sine and cosine integral functions given as [59]

$$\mathrm{Si}(x) = \int_0^x \frac{\sin t}{t} dt, \tag{42}$$

$$\mathrm{Ci}(x) = -\int_x^\infty \frac{\cos t}{t} dt. \tag{43}$$

Performing the integration in one of the equations (13)–(15), we obtain the Laplace transformation of the static dephasing magnetization decay, which can be written analogously to the cylindrical case (34) in the form

$$\hat{M}_0(s) = \frac{\rho}{1-\eta}\frac{1}{s}\left[H_S\left(\frac{s}{\eta\delta\omega}\right) - \eta H_S\left(\frac{s}{\delta\omega}\right)\right], \tag{44}$$

with the sphere-specific H function

$$H_S(y) = \frac{1}{3} + \frac{2}{3}\sqrt{\frac{1-iy}{3}}\left(1-\frac{2i}{y}\right)\mathrm{arccoth}\left(\sqrt{\frac{1-iy}{3}}\right). \tag{45}$$

We note that this sphere-specific H function is identical to the previously used function G [cf. Eq. (7) in [60]] with the inverse argument, i.e., $H_S(y)=G(1/y)$. Knowing the function H_S, we are able to obtain an analytical expression for the frequency density of states valid in all diffusion regimes. Applying the same steps as for cylinders, we eventually arrive at

$$p(\omega) = \frac{\tau_S}{\pi\rho}\left|\mathrm{Re}\,\frac{H_S\left(\frac{1+i\tau_S\omega}{\eta\tau_S\delta\omega}\right) - \eta H_S\left(\frac{1+i\tau_S\omega}{\tau_S\delta\omega}\right)}{\frac{1-\eta}{\rho}(1+i\tau_S\omega) - H_S\left(\frac{1+i\tau_S\omega}{\eta\tau_S\delta\omega}\right) + \eta H_S\left(\frac{1+i\tau_S\omega}{\tau_S\delta\omega}\right)}\right|. \tag{46}$$

Analogously to the case of cylinders, reflecting boundary conditions on the surface of the inner sphere are assumed to obtain the correlation time τ. Using the general expression in Eq. (5), we arrive at an expression for this case [cf. Eq. (27) in [43]]:

$$\tau_S = \frac{R_S^2}{2D(1-\eta)}\left[1 - \eta^{1/3} + \frac{4(1-\eta)^2 + 9(2\eta - \eta^{5/3} - \eta^{1/3})}{36(\eta^{5/3}-1)}\right]. \tag{47}$$

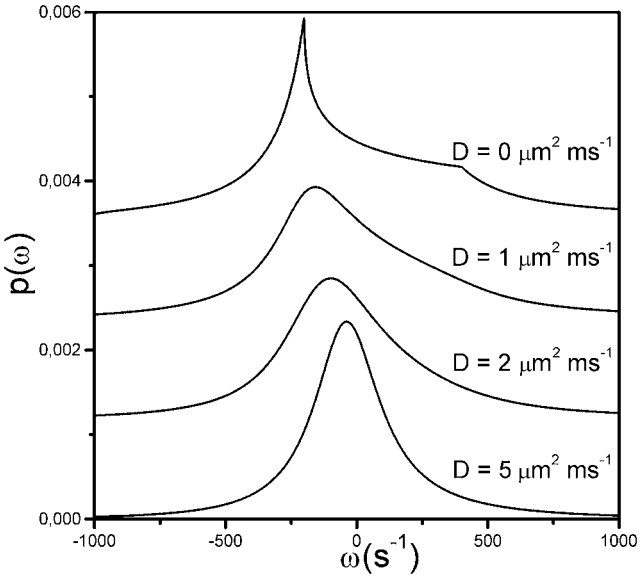

FIG. 7. Diffusion-dependent frequency density of states $p(\omega)$ for spheres obtained from Eq. (50) using the sphere H function given in Eq. (45). The parameters are volume fraction $\eta=0.2$, equatorial frequency shift $\delta\omega=1000\ \mathrm{s}^{-1}$, and radius $R_S=5\ \mu\mathrm{m}$.

To illustrate the dependence on the diffusion, the frequency density of states is shown in Fig. 7 for different values of the diffusion coefficient D. In the case of a vanishing diffusion coefficient, the frequency density of states coincides with the static dephasing frequency distribution given in Eq. (39) as shown in Fig. 1 of [34]. In the complimentary case of an increasing diffusion coefficient D which corresponds to the motional narrowing regime, the frequency distribution tends to a single-peaked narrow line shape as can be seen in Fig. 7.

A Fourier transformation of the frequency density of states $p(\omega)$ according to Eq. (16) leads to the magnetization decay as shown in Fig. 8. The spin-echo signal decay can be obtained from Eq. (22) and is shown in Fig. 9.

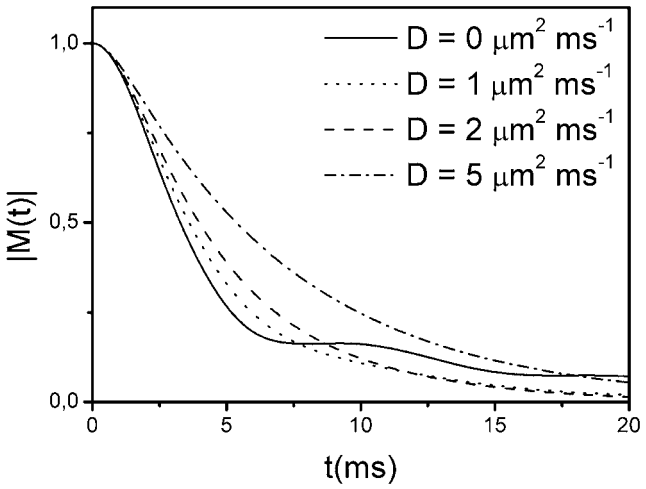

FIG. 8. Diffusion-dependent signal decay for spheres. The parameters are volume fraction $\eta=0.2$, equatorial frequency shift $\delta\omega=1000\ \mathrm{s}^{-1}$, and radius $R_S=5\ \mu\mathrm{m}$.

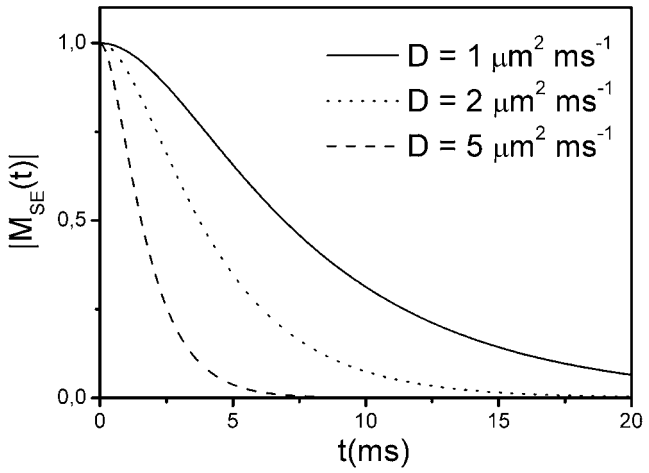

FIG. 9. Diffusion-dependent spin-echo signal decay for spheres. The parameters are volume fraction $\eta=0.2$, equatorial frequency shift $\delta\omega=1000\ \mathrm{s}^{-1}$, and radius $R_S=5\ \mu\mathrm{m}$.

C. General expressions

The assumption that the shape of the voxel arises from a central dilation of the magnetic inhomogeneity allows one to write the magnetization time evolution in the static dephasing regime according to Eq. (8) in the form

$$M_0(t)=\frac{\rho}{1-\eta}[h(\eta\delta\omega t)-\eta h(\delta\omega t)], \tag{48}$$

where the function h is dependent on the form of the inhomogeneity only. The existence and uniqueness of this function h is confirmed by using the fundamental theorem of calculus where lower and upper boundaries of the integral in Eq. (8) are the surface of the inhomogeneity and the surface of the voxel, respectively. In principle, the function h can be evaluated numerically or analytically. According to Eq. (2), the frequency shift $\delta\omega$ characterizes the strength of the magnetic perturber. Analogously to the signal time evolution, the Laplace transformation of this magnetization decay is given by

$$\hat{M}_0(s)=\frac{\rho}{1-\eta}\frac{1}{s}\left[H\left(\frac{s}{\eta\delta\omega}\right)-\eta H\left(\frac{s}{\delta\omega}\right)\right], \tag{49}$$

where the function H also depends on the form of the inhomogeneity only. Starting with Eq. (15), using the same arguments as before, H is the corresponding function to h in this case.

To find an expression for the frequency distribution, Eq. (21) has to be evaluated. Thus one eventually arrives at

$$p(\omega)=\frac{\tau}{\pi\rho}\left|\mathrm{Re}\,\frac{H\left(\frac{1+i\tau\omega}{\eta\tau\delta\omega}\right)-\eta H\left(\frac{1+i\tau\omega}{\tau\delta\omega}\right)}{\frac{1-\eta}{\rho}(1+i\tau\omega)-H\left(\frac{1+i\tau\omega}{\eta\tau\delta\omega}\right)+\eta H\left(\frac{1+i\tau\omega}{\tau\delta\omega}\right)}\right|. \tag{50}$$

This expression is the frequency density of states, which depends on the susceptibility effect (characterized by the frequency shift $\delta\omega$), the shape of the magnetized object (characterized by the function H), and the diffusion (characterized by the correlation time τ). Evaluating the general expression (5) as shown by [41,43,61], the correlation time exhibits the general expression for arbitrary shapes of the form

$$\tau=\frac{L^2}{D}k(\eta), \tag{51}$$

where L is the characteristic size of the magnetic inhomogeneity (i.e., the radius of the capillary or the sphere), D is the diffusion coefficient of the surrounding medium, and $k(\eta)$ is a function of the volume fraction η, where k depends on the shape of the magnetic inhomogeneity.

IV. EXPERIMENTAL VERIFICATION

To verify the analytical results experimentally it is necessary to obtain the exact form of the free induction decay caused by only the local magnetic field distortion of the susceptibility inhomogeneity. Hence, any kind of additional gradients such as imaging or shim gradients influences dramatically the form of the free induction decay and therefore its Fourier transformation, which corresponds to the frequency distribution. For this reason, gradient-echo sequences might cause significant deviation in the free induction decay time evolution, which hampers their application to this task. Another problem may arise from the fact that the frequency distribution often has a small bandwidth centered around the Larmor frequency $\omega_0=\gamma B_0$ caused by the external magnetic field. According to the Fourier theorem it is necessary to obtain the exact form of the free induction decay for long times to resolve the frequency interval in the immediate vicinity of ω_0. The strong signal decay for long times leads to a higher influence of the noise on the corresponding frequency interval for small frequencies. Hence, an appropriate method for quantification of the frequency distribution is the voxel-selective PRESS (point resolved spectroscopy) sequence [62,63]. Localization is achieved by three frequency-selective rf pulses (90°-180°-180°) in the presence of a B_0 magnetic field gradient. Signals outside the selected voxel are either not excited or not refocused, leading to a rapid

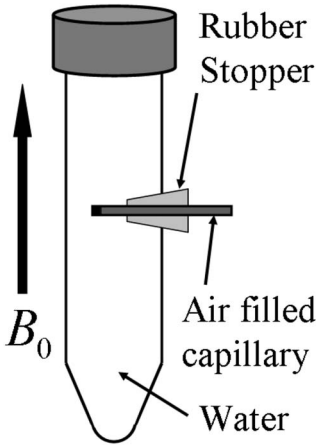

FIG. 10. Scheme of the phantom used for measuring the frequency distribution. The phantom was placed horizontally inside the magnet with the hole for the movable capillary on top. The hole for the capillary was sealed with rubber. The capillary was also sealed on the side within the water.

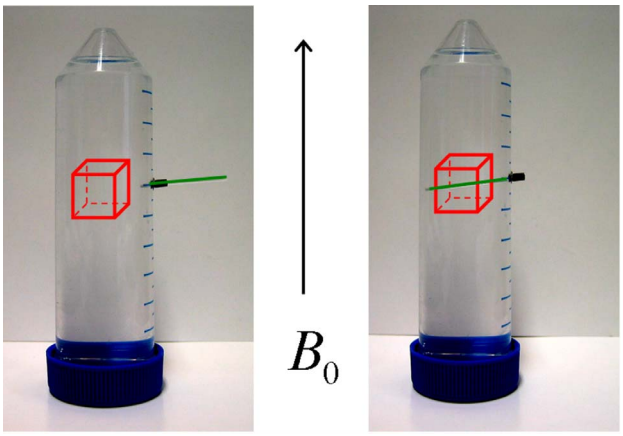

FIG. 11. (Color online) Left side: water-filled tube with capillary outside. The selected voxel was shimmed in this position. Right side: water-filled tube with capillary inside. In this position, the PRESS sequence was performed to measure the frequency distribution.

dephasing. Unwanted coherences induced by deviations from the nominal 180° nutation angles are dephased by the application of spoiler gradients surrounding the 180° pulses.

To avoid any unwanted influence of additional gradients, it is necessary to shim the voxel without the magnetic perturber. For this reason, we constructed a phantom which enables us to shim on the previously selected voxel to obtain a local Larmor frequency as close as possible to ω_0 throughout the whole voxel. Afterwards, the magnetic inhomogeneity has to be positioned into the voxel. This could be done without any displacement of the whole phantom to avoid any undesired distortion of the previously shimmed field inside the voxel. A phantom which fulfills these conditions is shown in Fig. 10. The voxel for shimming was selected larger than the voxel for measuring to avoid imperfect shim at the voxel boundaries. Furthermore, it was ensured that the capillary exceeds the boundaries of the voxel significantly to avoid distortions of the frequency distribution generated by its finite length and that it was oriented parallel to the voxel boundaries. A realization of this setup can be seen on the right side of Fig. 11.

It consists of a water-filled 50-ml centrifuge tube (Nunc GmbH & Co. KG, Thermo Fisher Scientific, Wiesbaden, Germany) with an inner diameter of 28 mm. On one side, a shiftable air-filled capillary with a diameter of $2R_C=1$ mm (glass No. 140, Hilgenberg GmbH, Malsfeld, Germany) was installed. This capillary, with negligible wall thickness, generates a susceptibility shift of $\Delta\chi=9$ ppm to the surrounding water.

The experiments were performed on a $B_0=7.05$ T Bruker Biospec system (Bruker BioSpin GmbH, Rheinstetten, Germany) equipped with actively shielded imaging gradients (397 mT/m maximum gradient strength) using a 72-mm quadrature birdcage resonator for rf transmission and receiving. The PRESS sequence was accomplished in a single scan with an echo time of $T_E=20$ ms. For exaction and refocusing, frequency-selective hermite shape pulses with a bandwidth of 5.4 kHz were used to select a voxel inside the tube. The free induction decay was recorded for 4.1 s at a bandwidth of 4 kHz, resulting in nominal spectral resolution of 0.24 Hz.

Utilizing the above described procedure (first selecting the voxel as shown on the left side of Fig. 11 and then inserting the capillary as shown on the right side of Fig. 11), we assured that only the susceptibility effects caused by the capillary influence the signal from the voxel. Because of the high sensitivity of the experiment on shimming, the size of the cuboid has a substantial influence on the quality of the measurement. In order to obtain analytical calculations we assumed that the capillary is surrounded by a cylindrical voxel as shown in Fig. 3. In the experiment a cuboid instead of a cylindrical voxel was used. The differences between the two shapes can be neglected in the case of a small volume fraction η. A too small size of the cuboid voxel results in a violation of this criterion $\eta \ll 1$ which justifies this replacement. A too large size of the cuboid voxel results in an imperfect shim of the magnetic field at the margins of the voxel. To find the optimal compromise between both requirements we selected a cuboid voxel with a size of 7.2 mm $\times 7.2$ mm $\times 7.2$ mm and performed the shim procedure when the capillary was outside the tube. This selection of the size of the cuboid voxel is optimal for the used parameters of the phantom. Thus, we obtain a volume fraction of $\eta=0.015$ for the size of this voxel which justifies the equivalence between a cuboid shaped voxel and a cylindrical voxel. Because of the horizontal orientation of the main magnetic field in the Biospec system, we were able to orientate the capillary perpendicular to the external field, i.e., $\theta=90°$, which maximized the susceptibility effect. To obtain the exact form of the free induction decay which is not influenced by any kind of gradients, we performed the PRESS sequence with the capillary inside the previously selected voxel (see Fig. 11).

According to Eq. (25) the capillary generates a frequency shift $\delta\omega_\theta=1341$ Hz in this experimental setup. With the known values for the frequency shift $\delta\omega_\theta$ and the volume

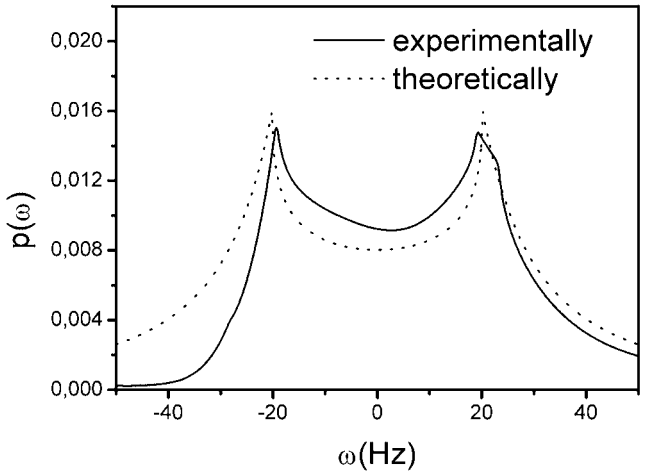

FIG. 12. Comparison of the experimentally obtained spectrum (solid line) with analytical result from Eq. (27) with the parameters η=0.015 and $\delta\omega_\theta$=1341 Hz (dashed line). As can be seen from Eq. (27), the characteristic peaks are at the positions $\pm\eta\delta\omega_\theta$, i.e., in our case at the positions ±20 Hz, which is also in good agreement with the experimental values.

fraction η we are able to compare the experimentally obtained spectrum with the predictions of Eq. (27). In Fig. 12 we see a very good agreement between the theoretically and experimentally obtained frequency distribution. Also, the free induction decay, for which we are able to give an analytical expression (28), is in good agreement with the experimentally obtained free induction decay as shown in Fig. 13. The frequency distribution around spheres was first considered by Cheng *et al.* [34]. Its experimental verification was performed by Seppenwoolde *et al.* [53] with similar phantoms and procedures as used in our experiments. Hereby, Fig. 7 in [53] is the corresponding figure for the spherical case to our Fig. 12 for cylindrical geometry. As can be seen

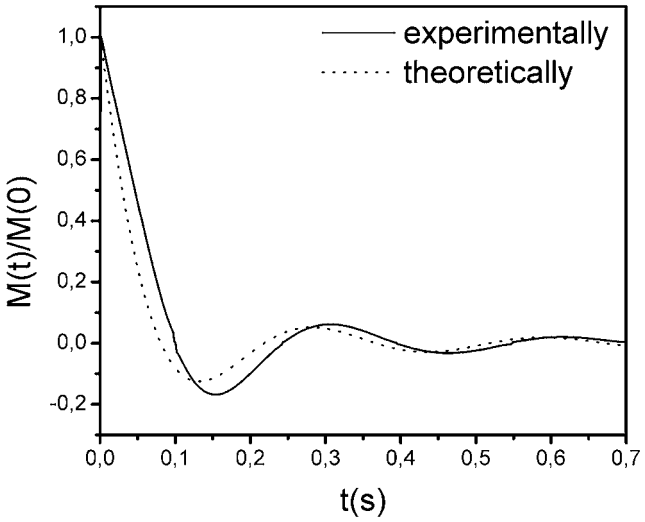

FIG. 13. Comparison of the experimentally obtained free induction decay (solid line) with analytical result from Eq. (28) with the parameters η=0.015 and $\delta\omega_\theta$=1341 Hz (dashed line).

in this publication, they also found good agreement for the frequency distribution around spheres between the measured and the analytical results of Cheng *et al.* [34].

V. SUMMARY AND CONCLUSIONS

At present, the frequency distribution of spins around a magnetic inhomogeneity is well understood in the static dephasing limit only. However analytical results are limited to special geometries such as spheres [34] or cylinders [9]. In this work, a formalism to describe the frequency distribution inside a voxel containing an arbitrarily shaped field inhomogeneity valid at the full range of diffusion regimes is developed.

The magnetic inhomogeneity creating the inhomogeneous field is denoted by the area G (cf. Fig. 1). It is surrounded by the dephasing volume containing diffusing spins. The diffusion process is characterized by the diffusion coefficient D. As shown in the above analysis, the shape of the inhomogeneity G, the magnetic strength $\delta\omega$ of the inhomogeneity, and the diffusion coefficient D alone determine the frequency distribution. It is important to remember that for high external magnetic field strengths, $\delta\omega$ depends on the saturation magnetization rather than on the susceptibility shift and the external magnetic field; i.e., hysteresis effects have to be taken into account in these cases. Thus, one finds $\delta\omega \propto \gamma\Delta M$ where ΔM is the difference in the magnetization of the inhomogeneity and the surrounding tissue [cf. Eq. (1) in [60]].

The form of the inhomogeneity G leads to the local frequency $\omega(\mathbf{r})$ around it [see Eq. (2)]. For the special cases of cylinders or spheres, this local frequency is given by a two-dimensional or three-dimensional dipole field [Eq. (26) or (38), respectively].

In Sec. II, the connection between the Laplace transformation of the magnetization time evolution and the frequency distribution is shown and used to derive a general expression for the frequency distribution valid in all diffusion regimes. In order to do this, a connection between the static dephasing regime and other diffusion regimes exploiting the Laplace transformation of the magnetization decay is used. This connection (7) was derived by Bauer *et al.* [6] using a *strong collision approximation*. This approximation represents a two-sided approximation of spin dephasing. It interpolates the relaxation process from very long (static dephasing regime) and short (motional narrowing regime) correlation times. Recently, this approximation was applied to describe the blood oxygen level dependent (BOLD) effect in myocardium [6] and the transverse relaxation of magnetically labeled cells [60]. To complement our previous work, this paper focuses on describing a formalism to understand the signal formation for general geometries and arbitrary pulse sequences. For example, now it is possible to describe the signal formation process of SPIO-labeled cells with SSFP sequences [64].

In this work, the general expression is analyzed treating the limiting cases of $\tau\rightarrow\infty$ (static dephasing regime) and $\tau\rightarrow 0$ (motional narrowing regime). Thus, it is possible to reobtain the well-known results of the static dephasing regime

for spheres and cylinders [9,34] and the motional narrowing regime.

The Bloch-Torrey equation has the form of the Schrödinger equation for imaginary time and with an imaginary potential in the Hamiltonian. Due to the imaginary potential, the Hamiltonian is non-Hermitian which hampers the development of a complete set of orthogonal eigenfunctions. Thus, the above method provides a practical method to solve the Bloch-Torrey equation at least in the *strong collision approximation*. Further analogies to quantum statistics arise from Eq. (11). The local Larmor frequency $\omega(\mathbf{r})$ corresponds to the dispersion relation of an excited ensemble (e.g., electron gas). In this picture, the diffusion constant D corresponds to the temperature and Eq. (21) is the generalization of Eq. (11) to finite temperatures.

Recalling the form of quadrupolar spin-1 powder line shape [65], we can see that the frequency distribution around a capillary in the case of small diffusion as shown in Fig. 4 looks similar to a first-order line shape as shown in Fig. 1 of [66] or a Pake doublet as shown in Fig. 4 of [67]. The same phenomenom occurs when comparing Fig. 7 with the second-order line shapes shown in Fig. 2.5b of [65]. On reflection, this is not surprising, since the Hamiltonian of the quadrupolar interaction [66] has a similar angle-dependent part to the local field around a capillary or to the local Larmor frequency in the case of dipolar interaction [68] has the same form as in the case of the sphere.

Basic experiments have been performed to test the analytical results. The good agreement of theoretical and experimental results shows that the setup generates a local resonance frequency that is sufficiently close to the ideal resonance frequency given in Eq. (26). Thus, if the assumption is that the capillary crosses the voxel completely, it is possible to obtain information about the volume fraction from the measured frequency distribution as stated in Eq. (20) and Fig. 3 in [9]. Because of the high sensitivity to shimming, these were very limited in varying parameters which influence the underlying diffusion regime. The experimental parameters imply measurements in the static dephasing regime due to the large capillary radius and the small diffusion coefficient which results in a long correlation time τ corresponding to a small dynamic frequency $1/\tau$. In further experiments, capillaries with smaller radius or higher diffusion coefficients could be used to decrease the correlation time and leave the static dephasing limit. Increasing the diffusion coefficient could be achieved by heating the surrounding water, but has to be done carefully to avoid convection. Besides this, slightly varying temperatures can lead to misadjustment of the shim. Also, adjusting other parameters like the characteristic frequency $\delta\omega$ or the volume fraction η should help to select the diffusion regime properties.

The theory could be further tested by performing an experiment with the response profile of an SSFP sequence [cf. Fig. 2 and Eq. (1)]. The appropriate method wold be a spectroscopic fast-acquisition double-echo (FADE) sequence [69] as previously used by Dreher *et al.* [70].

ACKNOWLEDGMENTS

This work was supported by the Schering Stiftung and the Deutsche Forschungsgemeinschaft-Sonderforschungsbereich 688 "Mechanismen und Bildgebung von Zell-Zell-Wechselwirkungen im kardiovaskulären System." We thank Jan-Henry Seppenwoolde, Jan Sedlacik, and Jürgen Reichenbach for stimulating discussions concerning the experimental verification and Stephan Glutsch for helpful comments concerning the numerical simulations.

APPENDIX: STRONG COLLISION APPROXIMATION

In this work, a central result of the strong collision approximation, especially Eq. (7), is used to obtain the local Larmor frequency distribution around field inhomogeneities valid for all diffusion regimes. Thus, a short review of the strong collsion approximation used throughout this paper is given in this appendix.

Discretizing the diffusion process, a jump dynamics between the different local Larmor frequencies can be introduced. This is realized by replacing the diffusion operator $D\nabla^2$ in Eq. (3) with a rate matrix $\mathbf{R}=(r_{ij})$, where the r_{ij} describes the transition rate of spins from a position with local Larmor frequency ω_i to a position with local Larmor frequency ω_j. If we assume that this transition probability depends only on the actual position of the spin, we can replace the diffusion process by a Markov process described by the generator $\mathbf{R}$. In this situation the time evolution of the spin is written in the form $\partial_t m_i(t)=\Sigma_j r_{ij} m_j(t)+i\omega_i m_i(t)$, where $m_i(t)$ is the transverse magnetization of a spin at a position with local Larmor frequency ω_i. The off-resonance frequencies caused by the field inhomogeneity can be written in matrix form $\mathbf{\Omega}=(\omega_i\delta_{ij})$. Introducing the vector $|m(t)\rangle$, where the ith element describes the transverse magnetization at Larmor frequency ω_i, we obtain a generalization of the Bloch-Torrey equation in operator form

$$\frac{\partial}{\partial t}|m(t)\rangle = (\mathbf{R} + i\mathbf{\Omega})|m(t)\rangle. \tag{A1}$$

In the original work of Torrey [18], diffusion processes were considered, i.e., $R=\nabla D(x)\nabla$, $\Omega=\omega(x)$, and $|m(t)\rangle=m(t)$ with the local Larmor frequency $\omega(x)$ and the local diffusion coefficient $D(x)$. Therefore, the original Bloch-Torrey equation (3) is a special case of the more general equation (A1). The formal solution of Eq. (A1) is given by $|m(t)\rangle=\exp[\mathbf{R}+i\mathbf{\Omega}]t|m(0)\rangle$.

The initial magnetization vector $|m(0)\rangle$ is proportional to the equilibrium eigenvector and thus $|m(0)\rangle\propto|0\rangle$. Normalizing the magnetization to unity [i.e., $\langle 0|m(0)\rangle=1$], the time evolution of the magnetization averaged over the complete dephasing volume can be calculated in the sense of Eq. (4):

$$M(t) = \langle 0|\exp[\mathbf{R} + i\mathbf{\Omega}]t|0\rangle. \tag{A2}$$

At this point, it is important to note that the generator of the stochastic process $\mathbf{R}$ is not Hermitian. Thus, the left eigenvector of $\mathbf{R}$ is not just the transpose of the corresponding right eigenvector of $\mathbf{R}$ as shown on p. 36 in [24].

To solve this general expression, we utilize a *strong collision approximation* [6,71]. The phrase "strong collision" has been used in many contexts by different authors. We

consider the strong collsion model in the sense of Dattagupta and Blume [72], which coincides with the model used by Lynden-Bell [73]. This approximation is adapted from statistical physics, where it is used to characterize Markov processes, i.e., processes where the initial and final states are stochastically independent and the transition probability between these states is proportional to the equilibrium probability of the final state. In the strong collision approximation, the generator of the stochastic process is replaced with the following form:

$$\mathbf{R} \underset{\text{collision}}{\overset{\text{strong}}{\longrightarrow}} \mathbf{D} = \lambda(\mathbf{\Pi} - \mathbf{1}), \tag{A3}$$

where $\mathbf{\Pi} = |0\rangle\langle 0|$ is the projection operator on the subspace spanned by the equilibrium eigenvector $|0\rangle$ of the generator $\mathbf{R}$. The operator $\mathbf{D}$ describes the diffusion as a stationary Markov process with a single rate λ that governs the dephasing of the steady-state distribution $p(\mathbf{r})$ independent of the initial state. Assuming the homogeneity of the surrounding tissue, the steady-state distribution is given by $p(\mathbf{r}) = 1/V$. Therefore, the application of the operator $\mathbf{\Pi}$ on some function $g(\mathbf{r})$ yields

$$\mathbf{\Pi} g(\mathbf{r}) = p(\mathbf{r}) \int_V d^3\mathbf{r} g(\mathbf{r}), \quad \mathbf{1} g(\mathbf{r}) = g(\mathbf{r}), \quad p(\mathbf{r}) = \frac{1}{V}. \tag{A4}$$

The identity operator is denoted by $\mathbf{1}$.

The fluctuation parameter λ in the approximation (A3) is the parameter which describes the time scale of the transitions in the Markov process. To determine this parameter we consider the correlation function $K(t)$ of the original diffusion process described by the Bloch-Torrey equation (3). This correlation function is defined as follows:

$$K(t) = \langle \omega(t)\omega(0)\rangle = \langle 0|\mathbf{\Omega} \exp[\mathbf{R}t]\mathbf{\Omega}|0\rangle. \tag{A5}$$

In terms of the original problem where the diffusion is described by the diffusion operator ($\mathbf{R} \to D\nabla^2$) and takes place in the local Larmor frequency [$\mathbf{\Omega} \to \omega(\mathbf{r})$], the correlation function can be written in the form

$$K(t) = \frac{1}{V} \int_V d^3\mathbf{r} \int_V d^3\mathbf{r}' \omega(\mathbf{r}) \exp[D\nabla^2 t] \omega(\mathbf{r}'). \tag{A6}$$

As shown in previous publications [6,43], it is possible to define a correlation time τ of a diffusing spin, which is determined in the context of a *mean relaxation time approximation* [74], as [6,43]

$$\tau := \int_0^\infty dt \frac{K(t)}{K(0)} \tag{A7}$$

and characterizes the time scale of the field fluctuations induced by molecular motion. Application of the correlation function of the original diffusion process given in Eq. (A6) to the mean relaxation time approximation (A7) yields the integral representation of the correlation time given in Eq. (5). To obtain this correlation time, it is assumed that diffusion takes place in the dephasing volume between the surface of the magnetic inhomogeneity and the surface of the voxel only. As shown in [41,43,61], this integration is straightforward and results in $\tau = L^2 k(\eta)/D$, where L is a characteristic length of the field inhomogeneity, i.e., the radius of a cylinder or a sphere. As shown in [41], the form function $k(\eta)$ also depends only on the shape of the inhomogeneity. The expression $(1/\nabla^2)\omega(\mathbf{r}) = c(\mathbf{r})$ in Eq. (5) is the solution of the inhomogeneous Laplace equation $\nabla^2 c(\mathbf{r}) = \omega(\mathbf{r})$ with the same boundary condition as the original Bloch-Torrey equation (3), which is possible since both differential equations are of the same type. The boundary conditions at the surface of the voxel as well as at the surface of the inhomogeneity provide the integration constants of the second-order differential equation. In this way, it is possible to incorporate the boundary conditions of the original problem in the strong collision approximation. For detailed discussion, see Eqs. (6) and (7) in [43].

To connect the fluctuation parameter λ with the correlation time τ, we replace the rate matrix $\mathbf{R}$ by its strong collision approximation $\lambda(\mathbf{\Pi} - \mathbf{1})$ in the definition of the correlation function, which yields $K(t) = \langle 0|\mathbf{\Omega} \exp[\lambda(\mathbf{\Pi} - \mathbf{1})t]\mathbf{\Omega}|0\rangle$. Inserting this expression of the correlation function into the definition of the correlation time, Eq. (A7), we eventually arrive at

$$\tau = \int_0^\infty dt \frac{\langle 0|\mathbf{\Omega} \exp[\lambda(\mathbf{\Pi} - \mathbf{1})t]\mathbf{\Omega}|0\rangle}{\langle 0|\mathbf{\Omega}^2|0\rangle} = \frac{1}{\lambda}. \tag{A8}$$

Hence, we are able to determine the time evolution of the magnetization $M(t)$ by applying the strong collision approximation (A3) with $\lambda = \tau^{-1}$ to the universally valid Eq. (A2), yielding

$$M(t) = \langle 0|\exp[\{\tau^{-1}(\mathbf{\Pi} - \mathbf{1}) + i\mathbf{\Omega}\}t]|0\rangle. \tag{A9}$$

Calculating the Laplace transformation of Eq. (A9) with the help of Eq. (6) yields

$$\hat{M}(s) = \langle 0| \frac{1}{\underbrace{(s + \tau^{-1})\mathbf{1} - i\mathbf{\Omega}}_{\mathbf{A}} \underbrace{-\tau^{-1}\mathbf{\Pi}}_{\mathbf{B}}} |0\rangle. \tag{A10}$$

Applying the operator identity $(\mathbf{A}+\mathbf{B})^{-1} = \mathbf{A}^{-1} - \mathbf{A}^{-1}\cdot\mathbf{B}\cdot(\mathbf{A}+\mathbf{B})^{-1}$ with abbreviations $\mathbf{A} = (s+\tau^{-1})\mathbf{1} - i\mathbf{\Omega}$ and $\mathbf{B} = -\tau^{-1}\mathbf{\Pi}$ to Eq. (A10), the Laplace transformation of the magnetization decay is found to be

$$\hat{M}(s) = \underbrace{\langle 0| \frac{1}{(s + \tau^{-1})\mathbf{1} - i\mathbf{\Omega}} |0\rangle}_{\hat{M}_0(s+\tau^{-1})} + \underbrace{\langle 0| \frac{1}{(s + \tau^{-1})\mathbf{1} - i\mathbf{\Omega}} |0\rangle}_{\hat{M}_0(s+\tau^{-1})} \tau^{-1} \underbrace{\langle 0| \frac{1}{s\mathbf{1} - \mathbf{R} - i\mathbf{\Omega}} |0\rangle}_{\hat{M}(s)}, \tag{A11}$$

where the subscript zero denotes quantities in the static dephasing regime, where the diffusion effects are neglected, i.e., $\mathbf{R} = \mathbf{0}$. Thus, the magnetization in the static dephasing

regime is given by $M_0(t)=\langle 0|\exp[i\mathbf{\Omega}]t|0\rangle$. Resolving Eq. (A11), we eventually obtain Eq. (7).

The statement of the stochastic independence of the initial and final states is closely connected with the assumption of an ergodic system. It means that the time scale of the field fluctuations determined by the diffusion process is significantly smaller than the time scale of the spin dephasing process. Only under this assumption the trajectory of the spin can cover nearly all possible local Larmor frequencies leading to the claimed stochastic independence of the intial and final states. Obviously, this demands strong diffusion, which is characterized by a large diffusion coefficient. Thus, the strong collision approximation works well in the motional narrowing regime. Besides this, in the calculation of the correlation time the full diffusion operator was taken into account. This leads to the correct dependence of the correlation time on the diffusion coefficient $\tau \propto D^{-1}$ for all diffusion regimes. Thus, we introduce the correct behavior for small diffusion coefficients and can extend the results of the strong collision approximation to the static dephasing regime.

To give a mathematical criterion for the applicability of the strong collision approximation, we write the local larmor frequency in the general form $\omega(\mathbf{r})=\delta\omega f(\mathbf{r})$; i.e., we seperate the the susceptibility properties from the form and size of the inhomogeneity as shown in Eq. (2) of [41]. Thus, we can write local larmor frequencies around a cylinder (26) in the form $\omega_C(\mathbf{r})=\delta\omega_\theta f_C(\mathbf{r})$ with the cylinder specific geometry function $f_C(\mathbf{r})=R_C^2\cos(2\phi)/r^2$. Analogously to Eq. (38), the sphere specific geometry function $f_S(\mathbf{r})=R_S^3(3\cos^2\theta-1)/r^3$ can be found. Using the expectation value $\langle f(\mathbf{r})\rangle = 1/V\int_V d^3\mathbf{r} f(\mathbf{r})$ of the geometry function $f(\mathbf{r})$, we can apply the condition $\Delta f(\mathbf{r})=\langle f^2(\mathbf{r})\rangle-\langle f(\mathbf{r})\rangle^2<(2\tau\delta\omega^2)^{-1}$ given in Eq. (29) of [41] to finally arive at $\eta\tau_C\delta\omega_\theta^2<1$ for cylinders and $\eta\tau_S\delta\omega^2<5/8$ for spheres. These inequalities can be viewed as mathematical criteria for the applicability of the strong collision approximation in these cases.

Diffusion processes in inhomogeneous magnetic fields were also treated by Kubo [cf. Eq. (6.28) in [24]]. The results of the strong collision approximation have a close connection to the line-shape theory of Kubo. To show this, we apply the Laplace transform to Eq. (A2) and substitute the result into Eq. (19), which finally yields

$$p(\omega)=\frac{1}{\pi\rho}\left|\mathrm{Re}\langle 0|\frac{1}{\mathbf{R}+i(\mathbf{\Omega}-\omega\mathbf{1})}|0\rangle\right|, \qquad \text{(A12)}$$

which is in agreement with the results of Kubo [cf. Eq. (6.25) in [24]]. Using the strong collision approximation, we were able to simplify this expression and obtain with Eq. (21) an applicable expression for the line shape at all diffusion regimes. Numerical results, by solving Eq. (A12) in the case of linear gradients $\omega(\mathbf{r})=\omega_0+\gamma Gz$, have been published by Pütz *et al.* [cf. Eq. (10) in [22]].

[1] S. Ogawa, T. M. Lee, A. R. Kay, and D. W. Tank, Proc. Natl. Acad. Sci. U.S.A. **87**, 9868 (1990).
[2] R. Weissleder, H. Cheng, A. Bogdanova, and A. Bogdanova, Jr., J. Magn. Reson Imaging **7**, 258 (1997).
[3] D. L. Kraitchman, A. W. Heldman, E. Atalar, L. C. Ammado, B. J. Martin, M. F. Pittenger, J. M. Hare, and J. W. M Bulte, Circulation **107**, 2290 (2003).
[4] A. Stroh, C. Faber, T. Neuberger, P. Lorenz, K. Sieland, P. M. Jakob, A. Webb, H. Pilgrimm, R. Schober, E. E. Pohl, and C. Zimmer, Neuroimage **24**, 635 (2005).
[5] R. M. Lebel, R. S. Menon, and C. V. Bowen, Magn. Reson. Med. **55**, 583 (2006).
[6] W. R. Bauer, W. Nadler, M. Bock, L. R. Schad, C. Wacker, A. Hartlep, and G. Ertl, Magn. Reson. Med. **41**, 51 (1999).
[7] W. R. Bauer, W. Nadler, M. Bock, L. R. Schad, C. Wacker, A. Hartlep, and G. Ertl, Phys. Rev. Lett. **83**, 4215 (1999).
[8] D. V. Baklanov, E. D. Demuinck, C. A. Thompson, and J. D. Pearlman, Magn. Reson. Med. **52**, 1438 (2004).
[9] C. H. Ziener, W. R. Bauer, and P. M. Jakob, Magn. Reson. Mater. Phy. (N.Y.) **18**, 225 (2005).
[10] K. Zhong, J. Leupold, J. Hennig, and O. Speck, Magn. Reson. Med. **57**, 67 (2007).
[11] E. M. Haacke, R. W. Brown, M. R. Thompson, and R. Venkatesan, *Magnetic Resonance Imaging: Physical Principles and Sequence Design* (Wiley, New York, 1999).
[12] R. Freeman and H. D. W. Hill, J. Magn. Reson. (1969-1992) **4**, 366 (1971).
[13] M. L. Gyngell, J. Magn. Reson. (1969-1992) **81**, 474 (1989).
[14] K. Scheffler and J. Hennig, Magn. Reson. Med. **49**, 395 (2003).
[15] A. Haase, J. Frahm, D. Matthaei, W. Hanicke, and K. Merboldt, J. Magn. Reson. (1969-1992) **67**, 258 (1986).
[16] H. Y. Carr, Phys. Rev. **112**, 1693 (1958).
[17] C. Ganter, Magn. Reson. Med. **56**, 687 (2006).
[18] H. C. Torrey, Phys. Rev. **104**, 563 (1956).
[19] S. D. Stoller, W. Happer, and F. J. Dyson, Phys. Rev. A **44**, 7459 (1991).
[20] V. G. Kiselev, J. Magn. Reson. **164**, 205 (2003).
[21] B. Pütz, D. Barsky, and K. Schulten, Chem. Phys. Lett. **183**, 391 (1991).
[22] B. Pütz, D. Barsky, and K. Schulten, J. Magn. Reson. (1969-1992) **97**, 27 (1992).
[23] D. Barsky, B. Pütz, and K. Schulten, Chem. Phys. Lett. **200**, 88 (1992).
[24] R. Kubo, *Fluctuations, Relaxation and Resonance in Magnetic Systems* (Oliver & Boyd, Edinburgh, 1962).
[25] R. Kubo, J. Math. Phys. **4**, 174 (1963).
[26] V. G. Kiselev and S. Posse, Phys. Rev. Lett. **81**, 5696 (1998).
[27] V. G. Kiselev and S. Posse, Magn. Reson. Med. **41**, 499 (1999).
[28] V. G. Kiselev and D. S. Novikov, Phys. Rev. Lett. **89**, 278101 (2002).
[29] A. L. Sukstanskii and D. A. Yablonskiy, J. Magn. Reson. **157**, 92 (2002).
[30] A. L. Sukstanskii and D. A. Yablonskiy, J. Magn. Reson. **163**, 236 (2003).

[31] A. L. Sukstanskii and D. A. Yablonskiy, J. Magn. Reson. **167**, 56 (2004).
[32] W. R. Bauer, C. H. Ziener, and P. M. Jakob, Phys. Rev. A **71**, 053412 (2005).
[33] W. R. Bauer and W. Nadler, Phys. Rev. E **65**, 066123 (2002).
[34] Y. C. Cheng, E. M. Haacke, and Y. J. Yu, Magn. Reson. Imaging **19**, 1017 (2001).
[35] D. A. Yablonskiy and E. M. Haacke, Magn. Reson. Med. **32**, 749 (1994).
[36] D. G. Norris, NMR Biomed. **14**, 77 (2001).
[37] S. C. Deoni, T. M. Peters, and B. K. Rutt, Magn. Reson. Med. **51**, 428 (2004).
[38] D. LeBihan, R. Turner, and J. R. Macfall, Magn. Reson. Med. **10**, 324 (1989).
[39] E. X. Wu and R. B. Buxton, J. Magn. Reson. (1969-1992) **90**, 243 (1990).
[40] R. Salomir, B. D. de Senneville, and C. T. W. Moonen, Concepts Magn. Reson., Part B **19**, 26 (2003).
[41] C. H. Ziener, T. Kampf, G. Melkus, P. M. Jakob, and W. R. Bauer, J. Magn. Reson. **184**, 169 (2007).
[42] T. Enss, S. Ahn, and W. S. Warren, Chem. Phys. Lett. **305**, 101 (1999).
[43] C. H. Ziener, W. R. Bauer, G. Melkus, T. Weber, V. Herold, and P. M. Jakob, Magn. Reson. Imaging **24**, 1341 (2006).
[44] K. T. Young, Magn. Reson. Imaging **21**, 451 (2003).
[45] C. J. G. Bakker, R. Bhagwandien, and M. A. Moerland, Magn. Reson. Imaging **12**, 767 (1994).
[46] L. D. Landau and E. M. Lifshitz, *Course of Theoretical Physics*, 3rd ed. (Pergamon, Oxford, 1999), Vol. 5.
[47] E. L. Hahn, Phys. Rev. **80**, 580 (1950).
[48] W. R. Bauer, W. Nadler, M. Bock, L. R. Schad, C. Wacker, A. Hartlep, and G. Ertl, Magn. Reson. Med. **41**, 1004 (1999).
[49] A. Krogh, J. Physiol. (London) **52**, 409 (1919).
[50] J. R. Reichenbach and E. M. Haacke, NMR Biomed. **14**, 453 (2001).
[51] F. Oberhettinger, *Tables of Bessel Transforms* (Springer-Verlag, Berlin, 1972).
[52] J. R. Zimmermann and M. R. Foster, J. Phys. Chem. **61**, 282 (1957).
[53] J. H. Seppenwoolde, M. van Zijtveld, and C. J. Bakker, Phys. Med. Biol. **21**, 361 (2005).
[54] T. A. Case, C. H. Durney, D. C. Ailion, A. G. Cutillo, and A. H. Morris, J. Magn. Reson. (1969-1992) **37**, 304 (1987).
[55] C. H. Durney, J. Bertolina, D. C. Ailion, R. Christman, A. G. Cutillo, A. H. Morris, and S. Hashemi, J. Magn. Reson. (1969-1992) **85**, 554 (1989).
[56] J. A. Bertolina, C. H. Durney, D. C. Ailion, A. G. Cutillo, A. H. Morris, and K. C. Goodrich, J. Magn. Reson. (1969-1992) **99**, 161 (1992).
[57] A. G. Cutillo, *Application of Magnetic Resonance to the Study of Lung* (Futura, Armonk, NY, 1996).
[58] C. V. Bowen, X. Zhang, G. Saab, P. J. Gareau, and B. K. Rutt, Magn. Reson. Med. **48**, 52 (2002).
[59] I. S. Gradstein and I. M. Ryshik, *Summen-, Produkt-und Integraltafeln/Tables of Series, Products, and Integrals* (Verlag Harry Deutsch, Thun, Frankfurt/Main, 1981).
[60] C. H. Ziener, W. R. Bauer, and P. M. Jakob, Magn. Reson. Med. **54**, 702 (2005).
[61] L. A. Stables, R. P. Kennan, and J. C. Gore, Magn. Reson. Med. **40**, 432 (1998).
[62] P. A. Bottomley, United States Patent No. 4, 480, 228 (1984).
[63] P. A. Bottomley, Ann. N.Y. Acad. Sci. **508**, 333 (1987).
[64] C. Heyn, C. V. Bowen, B. K. Rutt, and P. J. Foster, Magn. Reson. Med. **53**, 312 (2005).
[65] M. Mehring, *High Resolution NMR in Solids* (Springer-Verlag, Berlin, 1983).
[66] A. Jerschow, Prog. Nucl. Magn. Reson. Spectrosc. **46**, 63 (2005).
[67] D. D. Laws, H.-M. L. Bitter, and A. Jerschow, Angew. Chem., Int. Ed. Engl. **41**, 3096 (2002).
[68] B. Cowan, *Nuclear Magnetic Resonance and Relaxation* (Cambridge University Press, Cambridge, England, 1997).
[69] T. W. Redpath and R. A. Jones, Magn. Reson. Med. **6**, 224 (1988).
[70] W. Dreher, C. Geppert, M. Althaus, and D. Leibfritz, Magn. Reson. Med. **50**, 453 (2003).
[71] S. Dattagupta and M. Blume, Phys. Rev. B **10**, 4540 (1974).
[72] S. Dattagupta and M. Blume, Phys. Rev. A **14**, 480 (1976).
[73] R. M. Lynden-Bell, Mol. Phys. **22**, 837 (1971).
[74] W. Nadler and K. Schulten, J. Chem. Phys. **82**, 151 (1985).